JOURNAL OF APPLIED PHYSICS VOLUME 41, NUMBER 9 AUGUST 1970

Contact-Limited Currents in Metal–Insulator–Metal Structures*

T. C. McGill,† S. Kurtin,† L. Fishbone,‡ and C. A. Mead
California Institute of Technology, Pasadena, California 91109
(Received 26 September 1969; in final form 16 March 1970)

The physical mechanisms underlying current flow in solid-state MIM structures are reviewed with emphasis on criteria for determining the dominant conduction mechanism in a given experimental situation. Measurements of the bias and temperature dependence of currents through structures incorporating a thin film of single-crystal gallium selenide are reported, and are shown to be in excellent agreement with the predictions of a simple physical model of contact-limited emission. Independently measured properties of bulk single-crystal gallium selenide are used in all calculations; no adjustable parameters are employed. We believe that this study presents unequivocal evidence for contact-limited thermionic currents in solid-state MIM structures.

I. INTRODUCTION

In this paper we review the basic physics of contact-limited current flow and apply a simple model to the analysis of data obtained on well-defined MIM structures incorporating single-crystal gallium selenide as the thin insulating film. The bulk and interface properties of gallium selenide were determined by independent experiments; these properties were used in the calculation of theoretical currents. No adjustable parameters were required. Both the magnitudes and functional dependencies of observed currents are in excellent agreement with theoretical predictions. Experimental variables include voltage, temperature, and insulator thickness. We believe that the excellent quantitative agreement obtained between theory and experiment provides unequivocal evidence for thermionic contact-limited transport in solids.

Section II presents a brief perspective on the study of contact-limited currents. Section III reviews experimental data previously obtained on bulk gallium selenide. This data, in conjunction with the discussion of sample preparation of Section IV, is sufficient to fully describe the experimental specimens and hence to permit theoretical calculations of carrier transport phenomena without the need for curve fitting or the use of adjustable parameters. Section V discusses criteria for the observation of contact rather than bulk-limited currents and applies these criteria to our experimental specimens. Section VI discusses a simple theory of contact-limited thermionic currents and compares the results of numerical calculations with experimental data obtained on Al–GaSe–Au structures. Excellent agreement is noted. Section VII presents direct evidence for image-force (Schottky) barrier lowering. In addition, this section includes a discussion of the energy distributions of carriers contributing to contact-limited current flow. These distributions give insight into the physical mechanisms which yield contact-limited currents.

II. BACKGROUND

Contact-limited emission was first studied for the metal–vacuum interface. In this case three mechanisms of current flow may be distinguished:

(1) Thermionic emission[1] (Schottky emission) occurs in the low-field high-temperature limit and is a flux of electrons on the high-energy tail of the Maxwell–Boltzmann distribution over the image-force-lowered work-function barrier.

(2) Field emission[2,3] (Fowler–Nordheim tunneling) occurs in the high-field low-temperature limit and is the direct quantum mechanical tunneling of electrons from allowed states below the Fermi level in a metal into allowed states in the vacuum.

(3) Thermal–field emission[4–7] (T–F emission) occurs when the dominant contribution to the observed currents arises from the tunneling of thermally excited electrons through the narrow upper region of the image-force-lowered work-function barrier. This mechanism of current flow is intermediate between thermionic emission and field emission.

Murphy and Good[8] showed that each of these mechanisms is a limiting approximation observed under appropriate conditions of applied field and temperature. Therefore, it is not in general fruitful to classify contact-limited currents into these various mechanisms because a significant portion of an observed current–voltage characteristic may, in physical situations, arise from regions of crossover from one mechanism to the next. Moreover, analytic integration of the equation of current flow is not usually possible and hence numerical computation is used. To gain insight into the physics of carrier transport, one may also numerically evaluate the relative contribution to the current of carriers with various energies. Such energy distributions are considerably more informative than a mere classification of transport phenomena into the three cases outlined above.

Of course, even in metal–vacuum–metal structures, currents are not always contact limited. When more electrons are present in the vacuum region than can be collected in a transit time, buildup of free charge in the vacuum region leads to the familiar space-charge-limited conduction in which the virtual cathode is spatially displaced from the physical cathode.

As interest in solids developed, it was natural to attempt analysis of current flow in solid-state MIM structures. However, solid-state insulators are far more complex than a vacuum and many additional factors

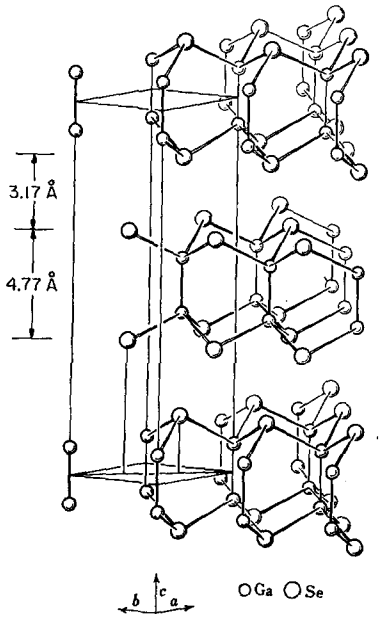

FIG. 1. Schematic representation of the layer compound GaSe (after H. Kumimura and K. Nahao, Ref. 13). The tightly bound fourfold (Se–Ga–Ga–Se) layers are 4.77 Å across and are held together at an interlayer separation of 3.17 Å by predominantly Van der Waals forces. This material cleaves easily perpendicular to its c axis thus facilitating the incorporation of a single-crystal film within a MIM structure.

must be taken into consideration. Two types of considerations arise:

(a) The fundamental parameters of the insulator (e.g., carrier effective mass and dispersion relationship, dielectric constants, mobility-field relationship, interface barrier energies, trap densities, and locations, etc.) must be known if meaningful predictions are to be made.

(b) Experimental techniques for preparing reproducible structures suitable for detailed study must be evolved.

These two types of considerations are not independent since values of the parameters used in theoretical treatments are often inferred from the results of measurements on experimental structures.

Samples are usually fabricated by oxidation of a deposited metal film or by similar techniques. These techniques yield amorphous insulating films whose properties are ill defined at best and are often spatially nonuniform. Current flow observed in such structures exhibits a generally exponential dependence on applied voltage and is often temperature dependent.[9–11] Since the bulk and interface properties of such insulating films are not known in detail, a rigorous matching of observed currents with a given model of carrier transport has not been possible. The usual procedure is to study the dependence of current on one or more variable (e.g., applied voltage, temperature, insulator thickness, electrode material, etc.), surmise an appropriate carrier transport mechanism or model, and then choose the parameters of the model (in fact these parameters are physical properties of the insulating film) so that the "predictions" of the model fit the observed currents. Great caution should be exercised when following such a procedure since physically distinct phenomena can lead to qualitatively similar behavior.[11] Even the distinctions between bulk and contact-limited current flow are blurred.[12] A real understanding of the underlying physics and its relevance to a given experimental situation can only be obtained from a detailed analysis of a well-defined experimental structure.

III. PROPERTIES OF GaSe

GaSe, used as the insulating material in all experiments reported here, is a layer compound having the crystal structure[13] shown in Fig. 1. This structure consists of tightly internally bound fourfold (Se–Ga–Ga–Se) layers, stacked one on top of another to form a macrocrystal held together by Van der Waals forces. As a result of this bonding configuration, it is possible to fabricate thin-film structures by peeling techniques in which the single-crystal character of the resulting GaSe thin film is maintained. Therefore, the properties of the GaSe film which is thus incorporated within a metal–GaSe–metal structure are necessarily identical with those of bulk GaSe crystals. The ability to incorporate a single-crystal thin film within MIM structures permits interface, bulk, and thin film measurements to be performed on one and the same well-defined material.

To characterize the bulk properties of GaSe, several experimental techniques have been employed. Dielectric constants have been determined by both low-frequency and infrared measurements.[14] Capacitance measurements on thin, fully depleted samples indicate the low-frequency dielectric constant $K_{dc}=8.0\pm0.3$ for the electric field parallel to the c axis ($\mathcal{E} \parallel c$). Analysis of infrared reflectivity for each polarization of the electric vector yields $K_{opt}=7.1$, $K_{dc}=7.6$ for $\mathcal{E} \parallel c$; and $K_{opt}=8.4$, $K_{dc}=10.2$ for $\mathcal{E} \perp c$. Multiple interference channeled spectra imply $K_{opt}=7.45$ and $K_{dc}=9.89$ for $\mathcal{E} \perp c$.

Experiments on metal–GaSe interfaces yield other important data. From measurements of capacitance as a function of voltage, our material was determined to be p type with $p=3\times10^{14}$ cm^{-3} at room temperature. Absorption edge measurements[15] indicate that the bandgap is 2.0 eV. In addition, photoresponse measurements at photon energies less than the bandgap yield surface barrier energies[16] (i.e., the energy of the metal Fermi level above the GaSe valence band): Al–GaSe, $\phi_{Al}=1.05$ eV; Au–GaSe, $\phi_{Au}=0.52$ eV.

The relative importance of trapping states in bulk GaSe samples was appraised by determining (at constant applied bias) the sensitivity to broad-band optical radiation of the capacitance of metal–semiconductor interfaces (Schottky barrier depletion layer). No measurable change in capacitance was observed for the

specimens used in this series of experiments. (Although material from highly doped ($p \simeq 10^{18}$ cm^{-3}) boules gave evidence of severe bulk trapping.) In addition, measurements of capacitance as a function of frequency, performed on these same interfaces, failed to reveal any lifetime-dependent phenomena. This evidence for the absence of dominant bulk trapping indicates that $N_T \ll p$.

Tunneling measurements performed on metal–GaSe–metal structures incorporating a GaSe film less than 100-Å thick indicate that the tunneling effective mass for carriers near the valence band edge is approximately 0.1 of the free electron mass. Data obtained from tunneling experiments are qualitatively different[17] from those for the thicker films discussed here and comprise an independent study which will be published elsewhere.[18]

IV. SAMPLE PREPARATION

Experimental structures used in this investigation were constructed by the following technique:

(1) Approximately 1000 Å of metal (typically aluminum) was vacuum evaporated on one side of a freshly cleaved GaSe flake ($\simeq 5$-μ thick).

(2) The flake was then mounted, metal side down, on a brass block. A 100% solids, silver-loaded epoxy was used both to bond the flake to the block and to provide electrical contact to the evaporated metal layer.

(3) The GaSe flake was peeled, in air,[19] to a thickness t (150 Å$<t<$2000 Å; i.e., 20–250 integral Se–Ga–Ga–Se layers) by application of a flexible adhesive tape (Scotch Magic Transparent Tape) to the exposed upper GaSe surface. Care was taken to assure that a continuous GaSe film was removed with each successive peeling step, thereby eliminating the possibility of gross surface contamination by the tape adhesive.

(4) Counterelectrodes of a metal (typically gold) were formed by vacuum evaporation through a fine mesh onto the freshly exposed (0001) surface. Each separate metallic dot defines an individual Al–GaSe–Au structure.

A schematic energy band representation of a typical (Al–GaSe–Au) structure is shown in Fig. 2. By virtue of the incorporation of a single-crystal thin film within the MIM sandwich, we are assured that the physical parameters of the structure are well defined. Since the GaSe films in our specimens are much thinner than the zero bias depletion layer thickness ($\simeq 1\ \mu$), the electric field within the structures is essentially uniform (in the absence of appreciable space charge, see Sec. V). Hence, Fig. 2 is an accurate energy band representation.

V. BULK LIMITATIONS

In the absence of direct tunneling between the metal electrodes, current transport through MIM structures involves two serial processes. Carriers are injected into the insulator at the metal–insulator interface; they then traverse the insulating region. Either process can in principle limit the current. However, it is possible to define some criteria which, if fulfilled, insure that bulk limitations are not dominant. Bulk-limited currents can arise via two mechanisms: space charge and scattering (including for our purposes shallow trapping and other processes yielding low effective mobility).

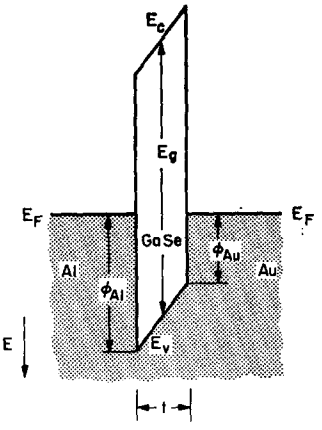

FIG. 2. Energy-band diagram of an Al–GaSe–Au structure under zero applied bias. Hole energy E increases down. E_g is the bandgap of GaSe, 2.0 eV. ϕ_{Al} is the Al–GaSe barrier energy, 1.05 eV; ϕ_{Au} is the Au–GaSe barrier energy, 0.52 eV. E_F denotes the Fermi level. As discussed in the text, this diagram is known to be accurate by virtue of the incorporation of a single-crystal GaSe film within the structure.

Space-charge limitations dominate carrier transport in MIM structures when the amount of uncompensated charge in the insulating region is sufficiently large to terminate a significant fraction of the field lines emanating from the metal electrodes. Both mobile charge (i.e., carriers in transit) and trapped charge contribute to this uncompensated charge. The mobile charge Q present in an insulator due to a current I is given by $Q=I\tau$, where τ is the time required for a charge carrier to transit the insulating film. If this charge is much less than the charge on the metal electrodes given by $Q(\text{electrode})=CV_T$, where C is the capacitance of the structure and V_T is the total voltage across the insulator (applied plus internal), then the space charge due to the mobile carriers is negligible. This condition is expressed by the inequality

$$I\tau < CV_T. \tag{5.1}$$

An upper bound on the contribution of trapped charge can be obtained from the total number of traps and the (worst case) assumption that all traps are ionized. Again, the criterion for neglecting the trapped space charge is that it be small compared to the total charge on the metal electrodes. The inequality

$$eN_tAt < CV_T, \tag{5.2}$$

where e is the electronic charge, N_t is the density of traps, t is the thickness of the insulator, and A is the area of the structure, expresses this condition.

In those cases where the charge carriers traverse the insulator against the field before encountering the limiting barrier, both trapping and strong scattering may lead to deviations from the simple ballistic model of current transport discussed below.

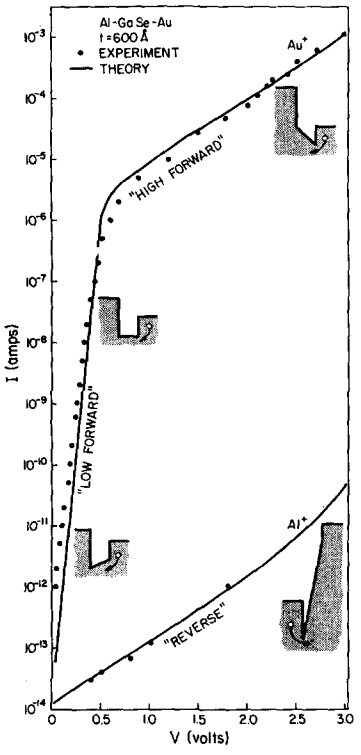

FIG. 3. Current–voltage characteristic of an Al–GaSe–Au structure. Both directions of applied bias are shown on this figure. The dots are experimental data; the solid line is numerically calculated from the theory of thermionic contact-limited currents [Eq. (6.3)] using parameters determined from prior experiments on bulk GaSe (no adjustable parameters were employed). Excellent agreement between theory and experiment is evident. The insets show partial band diagrams of the Al–GaSe–Au structure and illustrate the bias conditions we denote "low forward": $0<V<(\phi_{Al}-\phi_{Au})$; "flat band": $V=(\phi_{Al}-\phi_{Au})$; "high forward": $V>(\phi_{Al}-\phi_{Au})$; and "reverse": $V<0$. This descriptive notation is helpful when discussing thermionic contact-limited current flow because for a given structure it conveys a knowledge of the direction of current flow, the source metal, and the limiting barrier.

If none of these mechanisms for bulk current limitation is present, the current will be contact limited.

As noted in Sec. IV, the GaSe film incorporated within a Au–GaSe–Al structure is single-crystal material having the properties of bulk specimens. Thus, the criteria for observing contact- (as opposed to bulk) limited current can be checked in detail. For our material the number of traps is less than the acceptor density (as discussed in Sec. III), and hence, the effect of the space charge due to ionized acceptors and deep traps can be estimated from the acceptor density. For $p\sim 3\times 10^{14}$ cm^{-3} and $t\approx 500$ Å, the change in potential across the insulating layer due to ionized acceptors ($ept^2/2K_{opt}\epsilon_0$) is less than 10^{-3} eV. The influence of trapped charge on the barrier shape may thus be neglected.

The influence of space charge associated with current carriers in transit can be assessed on the basis of inequality (5.1). By using data from experimental current–voltage characteristics and the structure capacitance, we may estimate an upper limit (τ_{ub}) on the value of the transit time for which space-charge limitations are important, i.e., $\tau_{ub}=CV_T/I$. For a typical sample (the sample discussed in detail later in this section), τ_{ub} varies quite widely. However, (except for biases in the transition region from low forward to high forward where the field is nearly zero) the inequality is easily satisfied for physically reasonable values of effective carrier mobility. To illustrate this point, it is useful to express τ in terms of an effective mobility μ_{eff}: $\tau=t^2/\mu_{eff}V_t$ and to use the inequality $\tau<\tau_{ub}$ as a criterion for a lower bound (μ_{eff}^0) on the effective mobility. For μ_{eff} greater than this lower bound, charge associated with carriers in transit will not limit current flow. We find directly

$$\mu_{eff}^0=t^2I/CV_T^2. \tag{5.3}$$

For samples discussed in this paper t^2/C is of order one. Since μ_{eff}^0 becomes large for large I and small V_T, we will choose a "worst" case close to flat band: $V_T=0.1$ V, $I=10^{-6}$ A. Therefore, $\mu_{eff}^0\simeq 10^{-4}$ cm^2/V sec; a value much below that expected for this material even perpendicular to the layers. Therefore, currents observed in Au–GaSe–Al structures should be contact limited for all biases with the possible exception of forward biases within 0.1 V of $\phi_{Al}-\phi_{Au}$. Over this limited region the total internal field is small; space charge and other bulk limitations may be important.

VI. CONTACT-LIMITED TRANSPORT

A. Barrier Shape

An important consideration in any discussion of contact-limited current is the assumed shape of the barrier potential. Simple discussions assume the barrier to be trapezoidal in shape, neglect the influence of space charge in the insulator, and correct the barrier shape for single or multiple image charges induced in the metal electrodes. In this approximation, including multiple image charges, the barrier potential is given by[4]

$$\phi(x)=\phi_1+(\phi_2-\phi_1-V)(x/t)-(e/16\pi K_{opt}\epsilon_0 x)$$
$$-(e/8\pi K_{opt}\epsilon_0 t)\sum_{n=1}^{\infty}\{x^2/n[(nt)^2-x^2]\}, \tag{6.1}$$

where K_{opt} is the optical dielectric constant of the insulator; t is the thickness of the insulating layer, ϕ_1 and ϕ_2 are the barrier energies, and V is the applied voltage.[20] Except for the small range of biases where the electric field in the barrier region is very nearly zero, charge transport is limited by the energy barrier at one of the metal–insulator interfaces (i.e., the limiting barrier). Consequently, approximations to the barrier potential which are accurate near the limiting barrier are appropriate to the discussion of contact-limited current. For definiteness, let us take the limiting barrier to be ϕ_1, and hence consider Eq. (6.1) for x near zero. In

the appendix we show that in this region the multiple image-force correction [the fourth term in Eq. (6.1)] may be neglected to very good approximation.[21] Thus, Eq. (6.1) may be written

$$\phi(x)=\phi_0-\mathcal{E}x-(e/16\pi K_{\text{opt}}\epsilon_0 x), \qquad (6.2)$$

where we have introduced ϕ_0 for the limiting surface barrier energy and $\mathcal{E}$ for the total field acting near the limiting barrier.

B. Contact-Limited Current-Voltage Characteristics

In general, the total injection-limited current is the algebraic sum of four contributions: both holes and electrons may flow from either metal to the other. The relative importance of each of these contributions can be easily assessed using a simple thermionic model of carrier transport. To be specific, let us refer to the energy band diagram of Fig. 2 wherein the electrode materials are gold and aluminum. Consider the case in which a negative bias V is applied to the gold electrode. (Other bias conditions may be discussed in an analogous manner.) The hole current from Au to Al is proportional to $\exp[-(\phi_{\text{Al}}+V)/kT]$ while the hole current from Al to Au is proportional to $\exp(-\phi_{\text{Al}}/kT)$. Therefore, the ratio of the Au-to-Al hole current to the Al-to-Au hole current is equal to $\exp(-V/kT)$. Thus, for V greater than a few kT we can neglect the current contribution due to hole transport from Au to Al. Similarly, we find that for V greater than a few kT we can neglect the current contribution due to electron transport from Al to Au.

To assess the relative importance of hole current and electron current, we may use the same simple model. The dominant electron current is proportional to $\exp[-(E_g-\phi_{\text{Au}})/kT]$, where E_g is the bandgap of the insulator; the dominant hole current is proportional to $\exp(-\phi_{\text{Al}}/kT)$. Therefore, the ratio of hole current to electron current is given by $\exp[-(\phi_{\text{Au}}+\phi_{\text{Al}}-E_g)/kT]$. Thus, for $|\phi_{\text{Au}}+\phi_{\text{Al}}-E_g|>kT$ either hole or electron current must dominate. If $(\phi_{\text{Au}}+\phi_{\text{Al}}-E_g)>0$, elecron current dominates; if $(\phi_{\text{Au}}+\phi_{\text{Al}}-E_g)<0$, hole current dominates.

In summary, if both the applied bias and the quantity $|\phi_{\text{Au}}+\phi_{\text{Al}}-E_g|$ are greater than a few kT then the major contribution to the total injection limited current comes from one and only one of the four possible contributions. Throughout the remainder of this paper, the above criteria will be satisfied for applied biases greater than 0.05 V, since $|\phi_{\text{Au}}+\phi_{\text{Al}}-E_g|\sim 0.4$ eV$\gg kT$ ($kT\simeq 0.025$ eV at room temperature).

The current–voltage characteristic of an asymmetric ($\phi_{\text{Au}}<\phi_{\text{Al}}$) MIM structure in which current flow is contact limited depends on two factors: the source of the current carriers, and the barrier which limits current flow. These two factors lead to a natural division of the current–voltage characteristic into three distinct regions depending upon which energy barrier is limiting current flow and which metal is supplying most of the current carriers. As illustrated by the solid curves and insets of Fig. 3, these three distinct cases are "low forward," "high forward," and "reverse." Using the definition that positive bias results in current flow from gold to aluminum, we define the various cases in the following manner. Low forward occurs when positive bias is less than $\phi_{\text{Al}}-\phi_{\text{Au}}$. In this case the limiting barrier is the ϕ_{Al} barrier, the source of the current carriers is the gold electrode and current flows against the internal field. For the low forward, the current–voltage characteristic shows an exponential dependence of current on applied bias since the limiting barrier $(\phi_{\text{Al}}-V)$ decreases linearly with voltage. In the absence of scattering and direct-carrier tunneling, the slope of the $\log I$ vs V curve is very nearly $1/kT$. High forward occurs when the applied bias is positive and greater than $\phi_{\text{Al}}-\phi_{\text{Au}}$. In this case the limiting barrier is ϕ_{Au}, and the source of the current carriers is the gold electrode. Image lowering of ϕ_{Au} and contributions to the current from thermal-field and field-emission mechanisms cause the observed increases in current with increasing bias. Reverse occurs when the applied bias is negative. In this case the limiting barrier is ϕ_{Al}, and the source of the current carriers is the aluminum electrode. The increase in current with increasing bias observed in this case is a result of barrier lowering and tunneling, the same mechanisms which operate in the high forward.

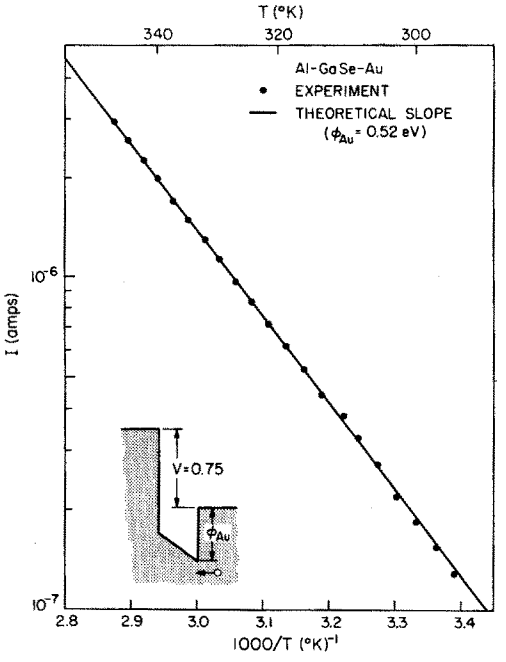

FIG. 4. Current as a function of $1000/T$ for a $V_{\text{Au}}=+0.75V$ (high forward) biased 600-Å-thick Al–GaSe–Au structure. The dots are experimental data; the solid line is calculated by numerical evaluation of Eq. (6.3) as a function of temperature. The correspondence between theory and experiment confirms the thermionic nature of current flow at the Au–GaSe interface.

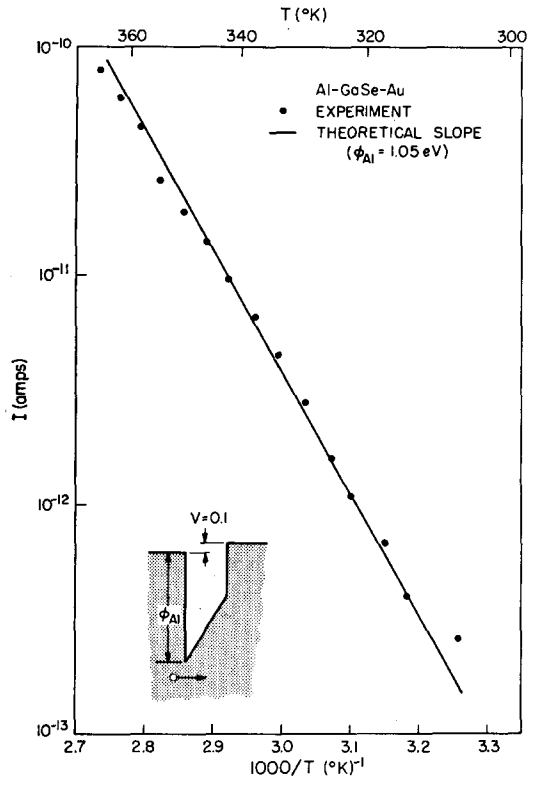

FIG. 5. Current as a function of $1000/T$ for a $V_{Al}=0.1V$ (reverse) biased 600-Å-thick Al–GaSe–Au structure. The dots are experimental data; the solid line is calculated by numerical evaluation of Eq. (6.3) as a function of temperature. The correspondence between theory and experiment confirms the thermionic nature of current flow at the Al–GaSe interface.

The solid curves of Fig. 3 are the theoretical current–voltage characteristic of an Al–GaSe–Au structure incorporating a 600-Å single-crystal film of GaSe. These curves were numerically calculated using the known properties of GaSe (see Sec. III) and a theoretical model (discussed below) of thermionic injection-limited currents adapted from the treatment by Murphy and Good[8,22] of the metal–vacuum interface.

In general, the expression for current as a function of applied voltage consists of the integral over all energies of two factors: a supply function which gives the flux of carriers from the source electrode, and a transmission function which gives the probability that a carrier incident on the limiting barrier is transmitted through it. In the approximation that the transmission function depends only on the component of the carrier's energy normal to the metal–insulator interface and on the applied bias (via the electric field $\mathcal{E}$), the current may be written as

$$I(V)=e\int dE\, P(E_\perp, V)N(E, V), \qquad (6.3)$$

where $E_\perp$ is the component of the carrier energy which is perpendicular to the plane of the interface and V is the applied bias. $P(E_\perp, V)$ and $N(E_\perp, V)$ are the transmission and supply functions, respectively. The limits on the integral in Eq. (6.3) are such that all the contributions to the current are taken into account. Following Murphy and Good,[8] we assume that the metal may be described[23] by a single parabolic band with effective mass m_m^*. In this case the supply function is given by[24,25]

$$N(E, V) = (4\pi m_m^*/\beta h^3) A \ln(1+\exp\{-\beta[E-E_F(V)]\}), \qquad (6.4)$$

where A is the area of the sample, E_F is the Fermi energy of the metal supplying the carriers,[26] and $\beta=1/kT$.

In determining the dependence of the transmission function on the perpendicular component of the energy two cases must be distinguished. In the first case, the carrier has a perpendicular energy which is greater than the maximum in the limiting barrier [Eq. (6.2)], and the transmission function (neglecting possible reflections at the interface[27]) is taken to be one. In the second case, the carrier has a perpendicular energy which is less than the maximum in the limiting barrier and must tunnel through a portion of this barrier if it is to contribute to the current. If the behavior of the carrier for energies lying inside of the forbidden gap is adequately described by an effective mass m_i^*, then following the derivation of Murphy and Good[8]

$$P(E_\perp, V)=[-\tfrac{2}{3}(m_i^*/\hbar^2)^{1/2}(e/\pi K_{opt}\epsilon_0)^{3/4}\mathcal{E}^{-1/4}y^{-3/2}v(y)], \qquad (6.5)$$

where $y=(e\mathcal{E}/4\pi K_{opt}\epsilon_0)^{1/2}/(\phi_0-E_\perp)$. Physically, y is the ratio of the image lowering of the barrier energy to the difference between the perpendicular component of the carrier energy and the surface barrier energy ϕ_0. The function $v(y)$ is given by[28]

$$v(y)=2^{-1/2}(1+a)^{1/2}\{\tilde{E}[2a/(1+a)]^{1/2} - (1-a)\tilde{K}[2a/(1+a)]^{1/2}\}, \qquad (6.6)$$

where $a=(1-y^2)^{1/2}$, and $\tilde{K}$ and $\tilde{E}$ are complete elliptic integrals of the first and second kind, respectively.

From the discussion of Secs. III–V, we know that our experimental structures correspond to the energy band diagram of Fig. 2 and hence that the previous discussion of the ideal MIM structures is directly applicable. We therefore expect that experimental current–voltage characteristics should correspond to the results of theoretical calculations based on this band diagram. The theoretical current–voltage characteristic (solid line) appearing in Fig. 3 has been calculated[29] for an Al–GaSe–Au structure 6.21×10^{-5} cm^2 in area and incorporating a GaSe film 600-A thick. The calculation is simply a numerical evaluation of Eq. (6.3) using the previously measured properties of bulk GaSe (see Sec. III). The solid black dots which also appear in Fig. 3 are data measured on a structure having a

gold counterelectrode area 6.21×10^{-5} cm^2 and incorporating a 600-Å-thick GaSe film. (Film thickness is determined directly from the electrode area and a measurement of structure capacitance at zero bias: $t=K_{dc}\epsilon_0 A/C$.) Excellent agreement between theory and experiment is evident from the figure. This agreement, in and of itself, gives strong support to the contact-limited transport model. Other predictions of this model must now be investigated.

C. Temperature Dependence

For external conditions such that both thermal-field emission and field emission are negligible the simple model of thermionic contact-limited current flow predicts that (at fixed applied bias) current should be exponentially dependent on temperature: $I\sim\exp(-\phi_0/kT)$, where ϕ_0 is the effective barrier energy limiting current flow. To confirm the thermionic origin of the currents observed in Al–GaSe–Au structures, it is necessary to experimentally check these predictions. Data obtained from such measurements are shown in Figs. 4 and 5. Values of applied bias were chosen such that current was limited either by the Al–GaSe barrier or by the Au–GaSe barrier.

From the inset of Fig. 4, it is clear that the slope of a line drawn through the data points in Fig. 4 should yield a value for the effective barrier height associated with the GaSe–Au interface. Evaluation of this experimental slope gives $\phi_0=0.514$ eV which differs only slightly from the 0.52 eV value found by photoresponse experiments performed on bulk specimens. This slight deviation is due to lowering of the effective barrier which results from both the image-force and thermal-field emission. For larger biases (higher fields) this effective lowering becomes even larger.

From the inset to Fig. 5, it is clear that the slope of the line of data points in Fig. 5 should yield a value for the effective barrier energy associated with the GaSe–Al interface. Evaluation of this slope gives $\phi_0=1.02$ eV, compared with the bulk photoresponse value of 1.05 eV. Image-force lowering (which is larger in this case than in the case discussed above because of the builtin field) accounts for a deviation of 0.046 eV.

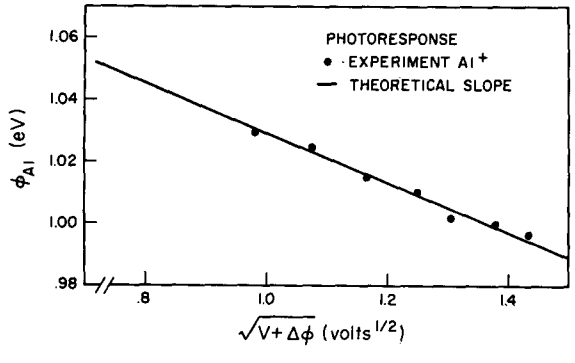

FIG. 6. Dependence of the effective Al–GaSe barrier energy on applied bias. To facilitate comparison with theoretical predictions of Schottky lowering [see Eq. (7.1)] the barrier energy ϕ_{Al} is plotted vs the square root of total internal bias: $V+(\phi_{Al}-\phi_{Au})$. The correspondence between theory and experiment confirms that the barrier energy exhibits Schottky lowering and is strong evidence that the barrier potential is, to good approximation, trapezoidal.

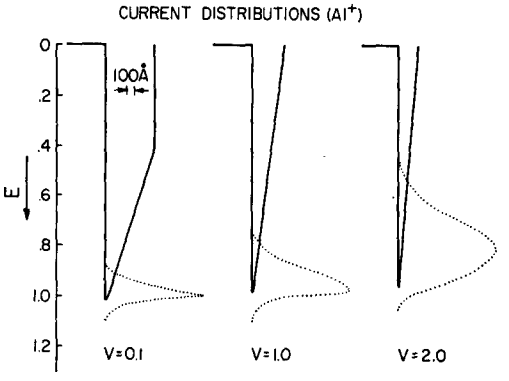

FIG. 7. Theoretical (normalized) current distribution for a reverse biased 600-Å-thick Al–GaSe–Au structure. The solid curves illustrate the shape of the image-force-lowered potential barrier; the dotted curves represent the distributions, as a function of hole energy E, of injected carriers. We note that the dominant injection mechanism shifts continuously with increasing bias from thermionic emission to thermally assisted tunneling. These curves have been calculated for the simple contact-limited current flow model discussed in the text. The validity of this model is assured by the previously discussed quantitative agreement between experiment and the predictions of this model.

For a comparison of observed behavior with detailed theoretical predictions, the solid lines plotted in both Figs. 4 and 5 were numerically computed directly from Eq. (6.3). This calculation takes into account the entire distribution of carriers and hence the theoretical curves in Figs. 4 and 5 deviate slightly from the perfectly straight lines predicted by a purely thermionic model. As evident from the figures, the agreement between theory and experiment is excellent. The correspondence between the barrier energies measured by photoemission experiments on bulk GaSe specimens and those measured thermally on MIM structures leaves no doubt concerning the thermionic origin of the observed currents, nor of their contact-limited nature.

VII. BARRIER SHAPE AND CARRIER DISTRIBUTION

A. Photoresponse Measurements

The photoresponse technique[30] is perhaps the best method of determining interface barrier energies on bulk specimens. We have applied this technique to MIM structures to directly investigate the electric field dependence of the interface barrier energy. Results of this investigation unambiguously established the barrier potential to be in fact as deduced in Sec. VI.

In the absence of appreciable tunneling,[31] photoresponse threshold (viz. ϕ_{photo}) is the energy difference between the Fermi level in the source metal and the maximum with respect of x of the barrier potential.

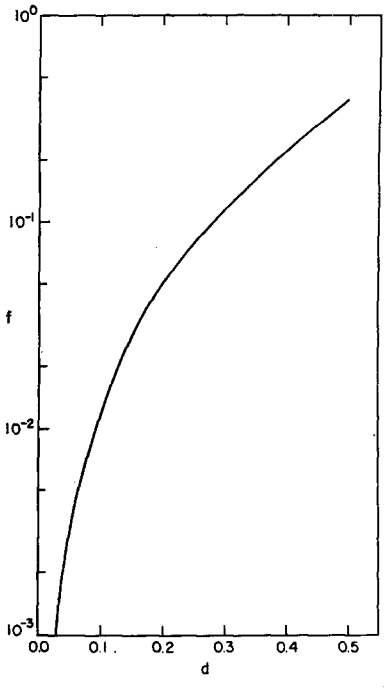

FIG. 8. Dependence of the function f (see Appendix) on the normalized distance d. This function measure the relative importance of the multiple image correction to the single image-force barrier lowering.

Solving Eq. (6.2) for its maximum yields

$$\phi_{\text{photo}} = \phi_0 - (e\mathcal{E}/4\pi K_{\text{opt}}\epsilon_0)^{1/2}. \tag{7.1}$$

This result is the well-known Schottky lowering in which the effective interface barrier decreases as the square root of the total field $\mathcal{E}$.

Data obtained from photoresponse measurements performed on the same structure whose current–voltage characteristic appears in Fig. 3 are presented in Fig. 6. For a given applied bias, the barrier energy ϕ_{Al} was obtained from the intercept of a plot of the square root of photoresponse per incident photon as a function of photon energy.[30] The voltage dependence of ϕ_{Al} was obtained directly from the Al^+ voltage dependence of photoresponse at fixed photon energy.[32] As shown in Fig. 6, this barrier energy exhibits the Schottky lowering predicted by the image-force correction to the barrier potential.

B. Carrier Distributions

Having thus established that the actual barrier potential is well described by the simple Schottky model, we can use the contact-limited transport theory of Sec. VI to gain insight into the detailed mechanisms of current flow.

Results of detailed numerical calculations, specifically for the case of the 600-Å-thick sample discussed above, are plotted in Fig. 7. For each applied bias the solid curves illustrate the actual image-force lowered barrier potential; the dotted curve represents the (normalized) relative contribution per unit energy to the current of carriers with a given value of $E_\perp$. The extent to which any given carrier injection mechanism contributes to the observed current under a specific set of external conditions can be seen directly. As illustrated by this figure, the dominant mechanism of current transport shifts continuously, with increasing internal field, from thermionic emission to field emission. For reverse bias >1.0 V, a large portion of the current is contributed by carriers tunneling through the upper portion of the image-lowered barrier.

VIII. CONCLUSION

Current flow in metal–insulator–metal structures is often very complex. In many cases physically distinct mechanisms can lead to qualitatively similar current–voltage characteristics. Interpretation of experimental observations is particularly difficult when the properties of the insulating layer are unknown. Hence, great care must be taken to avoid translating a lack of knowledge of the parameters of a structure into ambiguities about the physics of carrier transport. Many potential difficulties can be avoided if the parameters of an experimental structure are known from measurements which are independent of those performed to study current flow. With such a structure the physics governing current flow can be studied in detail because quantitative tests of the predictions of a given physical model are feasible.

In this study we have fabricated MIM structures containing single-crystal films of the layer compound gallium selenide. Prior experiments on bulk specimens of single-crystal gallium selenide provide data with which both the applicability and predictions of various models of current flow can be calculated. On the basis of such calculations we were able to deduce that space-charge limitations would be unimportant and to anticipate thermionic, contact-limited currents. Extensive measurements performed on the MIM structures are in excellent quantitative agreement with these calculations. We therefore believe that this study provides unequivocal evidence for contact-limited current flow in solids.

ACKNOWLEDGMENT

The authors would like to thank H. M. Simpson for constructing experimental apparatus employed in this series of experiments.

APPENDIX

Multiple image-force corrections to the barrier shape should be considered in a discussion of contact-limited current only if they significantly change the shape of barrier potential near that contact which is limiting the current. For samples with insulating layers which are thick enough to rule out the possibility of a significant contribution to the total current from direct tunneling

of carriers from one metal electrode to the other ($t \gtrsim 150$ A), and for electric fields which are large enough to define one barrier as the limiting barrier, the influence of multiple images is quite small. To illustrate this point consider the deviation $\Delta\phi(x)$ of the multiple image-force-corrected barrier potential from the single image-force-corrected barrier for x values near the limiting electrode. $\Delta\phi(x)$ is given by [see Eq. (6.1)]

$$\Delta\phi(x) = (e/8\pi K_{\text{opt}}\epsilon_0 t)f(d)$$
$$= (7.2 \text{ eV-Å}/K_{\text{opt}}t)f(d), \qquad \text{(A1)}$$

where

$$f(d) = \sum_{n=1}^{\infty} [d^2/n(n^2-d^2)], \qquad \text{(A2)}$$

and $d=x/t$. In Fig. 8 we have plotted $f(d)$ for d in the range 0–0.5 (for d greater than 0.5, we should correct the barrier shape for the image in the second electrode). This figure demonstrates that $f(d)$ is less than one throughout the range of d from 0 to 0.5. Thus, a crude upper bound for the contribution of multiple images to the barrier shape can be obtained by evaluating the numerical factor multiplying $f(d)$ in Eq. (A1) for typical values of $K_{\text{opt}}(=7)$ and $t(=200$ Å); this yields

$$\Delta\phi < 3.6\times10^{-3} \text{ eV}. \qquad \text{(A3)}$$

This estimate is very conservative. Values of d which are important in determining the current are frequently less than 0.5. Hence, a more appropriate bound of $f(d)$ would be between 10^{-2} and 10^{-1}. We conclude that for all cases discussed herein, the effect of multiple image-force corrections to the barrier shape is negligible.

* This work supported in part by the Office of Naval Research.
† Howard Hughes Doctoral Fellow.
‡ Presently at the University of Maryland, Department of Physics, College Park, Md. 20742.

[1] W. Schottky, Z. Physik **15**, 872 (1914).
[2] L. W. Nordheim, Proc. Roy. Soc. (London) **A121**, 626 (1928).
[3] R. H. Fowler and L. W. Nordheim, Proc. Roy. Soc. (London) **A119**, 173 (1928).
[4] A. Sommerfeld and H. Bethe, *Handbuch der Physik*, edited by H. Geiger and K. Scheel (Springer, Berlin, 1933), Vol. 24, No. 2.
[5] E. Guth and J. C. Mullin, Phys. Rev. **61**, 339 (1942).
[6] W. W. Dolan and W. P. Dyke, Phys. Rev. **95**, 327 (1954).
[7] W. P. Dyke, J. P. Barbour, E. E. Martin, and J. K. Trolan, Phys. Rev. **99**, 192 (1955).
[8] E. L. Murphy and R. H. Good, Phys. Rev. **102**, 1464 (1956).
[9] P. R. Emtage and W. Tantraporn, Phys. Rev. Lett. **8**, 267 (1962).
[10] C. A. Mead, Phys. Rev. **128**, 2088 (1962).
[11] J. J. O'Dwyer, J. Appl. Phys. **37**, 599 (1966).
[12] See for example: J. G. Simmons, Phys. Rev. Lett. **15**, 967 (1965); P. Mark and T. E. Hartman, J. Appl. Phys. **39**, 2163 (1968).
[13] H. Kamimura and K. Nahao, J. Phys. Soc. Japan **24**, 1313 (1968).
[14] P. C. Leung, G. Anderman, W. G. Spitzer, and C. A. Mead, J. Phys. Chem. Solids **27**, 849 (1966).
[15] P. Fielding, G. Fisher, and E. Mooser, J. Phys. Chem. Solids **8**, 434 (1959).
[16] S. Kurtin and C. A. Mead, J. Phys. Chem. Solids **29**, 1865 (1968).
[17] G. Lewicki and C. A. Mead, Phys. Rev. Lett. **16**, 939 (1966).
[18] S. Kurtin and C. A. Mead (unpublished).
[19] Previous work indicates that surface barriers prepared on GaSe are not sensitive to whether the GaSe is cleaved in vacuum or in air (see Ref. 16).
[20] All energies and potentials throughout this discussion are measured in electron volts. All other units are mks.
[21] The appendix defines criteria for neglecting the multiple image-force correction. For a detailed discussion of various approximations to the multiple image-force correction, see J. G. Simmons, J. Appl. Phys. **39**, 1793 (1963).
[22] Such adaptation has been previously discussed by several authors. See for example: W. Tantraporn, Solid-State Electron. **7**, 81 (1964); R. Stratton, Solid-State Electron. **8**, 175 (1965).
[23] The question of what effective mass to use has been discussed by several authors. See for example: Ref. 21 and also C. Crowell, Solid-State Electron. **8**, 395 (1965). Since small deviations in the value of pre-exponential factors do not affect the qualitative character of the physics being studied we choose to use a conceptually simple model uncluttered by experimentally indeterminate quantities.
[24] R. Fowler and E. A. Gugenheim, *Statistical Thermodynamics* (Cambridge U. P., New York, 1952), p. 460.
[25] In the low forward [see Fig. 3(b)] carriers traverse the insulating region against the electric field before encountering the limiting barrier. Hence, for the low forward, the assumed form of the supply function may be in error because both scattering of carriers within the insulator and reflection at the metal–insulator interface have been neglected. These effects may be responsible for the slight deviation of calculated currents from those experimentally observed in the low forward.
[26] The voltage dependence of the Fermi energy indicated in Eq. (6.4) calls attention to the possible variation of this energy with respect to the defined energy zero. For example, in the forward the energy zero is taken at the Fermi level of $M2$; the Fermi level of the source metal ($M1$) varies with respect to the energy zero as the applied bias is changed.
[27] Recently some authors have addressed themselves to the problem of correcting for reflections at the metal–semiconductor interface (in Schottky barrier diodes). See for example C. R. Crowell and S. M. Sze, J. Appl. Phys. **37**, 2683 (1966); C. R. Crowell, Solid-State Electron. **8**, 395 (1965); **12**, 55 (1969). However, since reflection leads only to a change in the prefactor multiplying the current, experimental attempts to verify the modification due to reflection have proven to be exceedingly difficult.
[28] R. E. Burgess and K. Kroemer, Phys. Rev. **90**, 515 (1953).
[29] The effective mass of electrons in either metal is taken to be one throughout these calculations.
[30] C. A. Mead, Solid-State Electron. **9**, 1023 (1966), and the references contained therein.
[31] The role of tunneling near the top of the image-force lowered potential barrier may be assessed by computation of the quantum mechanical transmission coefficient as a function of energy (referenced to ϕ_{photo}). As long as the energy range over which a significant number of the incident carriers can tunnel through the barrier is small compared with the energy range over which photoresponse measurements are made, the primary effect of tunneling will be to contribute a "tail" to the photoresponse data. If this tail is ignored, the barrier energy measured by photoresponse will be ϕ_{photo}.
[32] F. A. Padovani, Rev. Sci. Instrum. **39**, 772 (1968).